Co-binding of pharmaceutical compounds at mineral surfaces: Molecular investigations of dimer formation at goethite/water interfaces

Jing Xu, Remi Marsac, Dominique Costa, Wei Cheng, Feng Wu, Jean-François Boily, Khalil Hanna

Article

Co-binding of pharmaceutical compounds at mineral surfaces: Molecular investigations of dimer formation at goethite/water interfaces

Jing Xu, Rémi Marsac, Dominique Costa, Wei Cheng, Feng Wu, Jean-François Boily, and Khalil Hanna

Environ. Sci. Technol., **Just Accepted Manuscript** • DOI: 10.1021/acs.est.7b02835 • Publication Date (Web): 03 Jul 2017

Co-binding of pharmaceutical compounds at mineral surfaces: Molecular investigations of dimer formation at goethite/water interfaces

Jing Xu [a,b], Rémi Marsac [b #], Dominique Costa [c], Wei Cheng[b], Feng Wu [d], Jean-François Boily [e], Khalil Hanna [b]*

[a]State Key Laboratory of Water Resources and Hydropower Engineering Science, Wuhan University, Wuhan 430072, China

[b]Ecole Nationale Supérieure de Chimie de Rennes, CNRS, UMR 6226, 11 Allée de Beaulieu, CS 50837, 35708 Rennes Cedex 7, France.

[c]Institut de Recherches de Chimie de Paris UMR 8247 ENSCP Chimie Paristech, 11 rue P. Et M. Curie, 75005 Paris, France.

[d]Hubei Key Lab of Biomass Resource Chemistry and Environmental Biotechnology, School of Resources and Environmental Science, Wuhan University, Wuhan, 430079, P. R. China.

[e]Department of Chemistry, Umeå University, Umeå, SE-901 87, Sweden

*Corresponding author: Tel.: +33 2 23 23 80 27, khalil.hanna@ensc-rennes.fr

[#]Present address: Géosciences Rennes, UMR CNRS 6118, Université de Rennes 1, Campus de Beaulieu, CS74205, 35042 Rennes Cedex, France

A manuscript re-submitted to *ES&T*

June, 2017

Abstract

The emergence of antibiotic and anti-inflammatory agents in aquatic and terrestrial systems is becoming a serious threat to human and animal health worldwide. Because pharmaceutical compounds rarely exist individually in nature, interactions between various compounds can have unforeseen effects on their binding to mineral surfaces. This work demonstrates this important possibility for the case of two typical antibiotic and anti-inflammatory agents (nalidixic acid (NA) and niflumic acid (NFA)) bound at goethite (α-FeOOH) used as a model mineral surface. Our multidisciplinary study, which makes use of batch sorption experiments, vibration spectroscopy and periodic density functional theory calculations, reveals enhanced binding of the otherwise weakly bound NFA caused by unforeseen intermolecular interactions with mineral-bound NA. This enhancement is ascribed to the formation of a NFA-NA dimer whose energetically favoured formation (-0.5 eV compared to free molecules) is predominantly driven by van der Waals interactions. A parallel set of efforts also showed that no co-binding occurred with sulfamethoxazole (SMX) because of the lack of molecular interactions with co-existing contaminants. As such, this article raises the importance of recognising drug co-binding, and lack of co-binding, for predicting and developing policies on the fate of complex mixtures of antibiotics and anti-inflammatory agents in nature.

Introduction

Thousands of different emerging pharmaceutical contaminants occur in soils, groundwater, surface waters as well as seawater from human and intensive farming activities.[1,2] Antibiotics and anti-inflammatory agents in terrestrial and aquatic environments, in some instances at levels as high as several hundred ng per L [3–6] are posing detrimental ecological and health effects especially because of their growing use in human and veterinary medicine. Because the fate of these compounds is often tied to their affinities to surfaces of soil and sediment mineral particles [7,8], adsorption through synergistic drug interactions is likely to become an emerging mechanism in contaminated environments.

Although contaminants rarely exist in isolation, they often have been studied individually with respect to sorption and/or complexation with naturally occurring minerals.[9–12] Sorption of individual compounds to environmental surfaces involves different mechanisms including metal bond, hydrogen bond, and van der Waals interactions [13]. In multicomponent systems, co-existing contaminants can compete for surface binding sites, or cooperatively bind by co-neutralisation of surface charge and/or by direct molecular interactions. While competitive adsorption has been widely investigated[14–16], cooperative effects have been never reported for widely used antibiotic and anti-inflammatory agents. In addition, because most traditional environmental models are based on an individual contaminant basis, little is known on their fate in mixed contaminant systems.

In this work, we assessed the ability of three typical antibiotic and anti-inflammatory agents detected in affected environments[6,17] (nalidixic acid (NA), niflumic acid (NFA) and sulfamethoxazole (SMX)) to co-bind at minerals surfaces. Goethite (α-FeOOH) is selected as model mineral because it is one of the most stable thermodynamically iron oxyhydroxide at ambient temperature and the most abundant one in natural settings. NA is a quinolone antibiotic that is widely used in humans and animals and that typically co-occurs with SMX, a sulfonamide antibiotic commonly used to treat a variety of bacterial infections[18]. Niflumic acid (NFA) is a non-steroidal anti-inflammatory that is often used for rheumatoid arthritis.[19] As will be detailed in this work, investigations are mainly focused on NA and NFA as no co-binding effect are typically observed with SMX. Vibration spectroscopic and density functional theory (DFT) calculations of NA/NFA co-binding, as well as batch kinetic, pH-edges and isotherms, were used to resolve uptake mechanisms of NA and NFA at goethite in isolated *vs.* mixed systems. These efforts helped identify conditions under which drug co-binding is likely to prevail in the environment.

Experimental Methods

Materials and chemicals. Nalidixic acid (NA), Niflumic acid (NFA), Sulfamethoxazole (SMX), sodium chloride (NaCl), potassium hydroxide (KOH), sodium hydroxide (NaOH) and hydrochloric acid (HCl) were obtained from Sigma Aldrich, and were of analytical grade or better. The preparation and characteristics of goethite are detailed in the supporting information (SI).

Binding and co-binding experiments

Kinetic adsorption experiments were conducted in 125 mL Nalgene bottles containing 0.5 g/L goethite in 10 mM NaCl under an atmosphere of N_2(g). NA, NFA and SMX concentrations were of 20 μM in both isolated (NA; NFA; SMX) and mixed (NA+NFA; NA+SMX, NFA+SMX) systems. pH was adjusted using dilute NaOH or HCl solutions to a pre-selected value. Aliquots were sampled during the course of the experiments and filtered (0.2 μm) for analysis. Preliminary experiments showed that adding the ligand simultaneously or sequentially after several hours of equilibration had no significant effects on adsorption results.

Equilibrium adsorption experiments as a function of pH ($4 < pH < 9$) were conducted in 15 mL polypropylene tubes under an atmosphere of N_2(g) to minimize interferences with dissolved CO_2 at $pH > 6.5$ (Fig. S1). Adsorption isotherms were, in turn, recorded at pH = 6 under N_2(g) for (i) equimolar concentrations of NA and NFA (0.1 - 40 μM), (ii) $[NA]_{tot}$ = 20 μM and varying $[NFA]_{tot}$ (0.1 - 40 μM), and (iii) $[NFA]_{tot}$ = 20 μM and varying $[NA]_{tot}$ (5 - 40 μM). The adsorbed amount was calculated by depletion method. Desorption tests were also conducted at pH = 11 to check the mass balance, and an average recovery of 99±2% for the investigated solutes was obtained (see SI). Sorption and desorption experiments were performed at least twice, and the reproducibility of the measurements was around 5% for NA and 10% for NFA.

Aqueous concentrations of organic molecules were determined using a high performance liquid chromatography (Waters 600 Controller) equipped with a

reversed-phase C18 column (250 mm×4.6 mm i.d., 5 μm) and a photodiode array detector (Waters 996). The mobile phase was mixture of acetonitrile/water (60/40v/v) contained 0.1% formic acid. The flow rate was set at 1 mL/min in isocratic mode. The detector was set to 258 nm for NA, 283 nm for NFA and 270 nm SMX. All three molecules could be analyzed with a single injection because they exhibited different retention times (NA: 4.5 min; NFA: 10.1 min; SMX: 3.2 min).

ATR-FTIR spectroscopy and MCR analysis

Attenuated total reflectance-Fourier transform infrared (ATR-FTIR) spectra were recorded between in the 780-4000 cm^{-1} region on an IS50 Nicolet spectrometer equipped with a KBr beam splitter and a liquid nitrogen cooled MCT detector. A nine-reflection diamond ATR accessory (Durasampl*IR* ™, Sens IR Technologies) was used for acquiring spectra of wet samples. The resolution of the single beam spectra was 4 cm^{-1}.

Sample preparation for the ATR-FTIR analysis was the same as for batch sorption experiments and has described in detail in our previous work[20]. Spectra of goethite suspensions in 10 mM NaCl were also taken in the absence of NA and NFA and then subtracted from the spectra of sorbed NA and/or NFA in order to represent surface complexes only. Two series of experiments were conducted at pH=6 in 10 mM NaCl for 0.5 g/L goethite and (i) $0 < [NFA]_{tot} < 100$ μM with $[NA]_{tot} = 100$ μM or (ii) $0 < [NA]_{tot} < 100$ μM with $[NFA]_{tot} = 100$ μM. Due to the relatively low solubility of both NA and NFA (see SI), 1 M NaOH was used to dissolve NA or NFA to ensure a high

concentration (10 mM) for ATR-FTIR analysis of NA and NFA aqueous solution. The solid form of NA and NFA was also analysed using ATR-FTIR by loading powder on the crystal, and then a drop of water was added to apply it more uniformly. Additionally, the effect of pH (4-6) on NA and NFA sorption to goethite in 10 mM NaCl was investigated for $[NA]_{tot}$ or $[NFA]_{tot}$=100 μM as described in supporting information (SI).

Selected sets of ATR-FTIR spectra in the 1200-1700 cm^{-1} region were then analyzed by multivariate curve resolution (MCR) analysis[21]. These efforts extracted spectral profiles and their relative concentrations (FTIR measurements cannot be used to obtain absolute concentration values) of end-member components representing an assemblage of the purest chemical species possible. Spectra sets were expressed in the matrix **A** (*m* rows of wavenumber and *n* columns of measurements), and offset to zero absorbance at 1700 cm^{-1}, where absorption by the wet mineral pastes is constant. The spectra were expressed in terms of a linear combination of spectral profiles (**ε**), akin to molar absorption coefficients, and their concentration profiles (**C**), and are related by **A**= **εX** as in the Beer-Lambert law, such that that **ε**≥0 and **C**≥0. Calculations of **ε** and **C** were made with the MCR-ALS program[21] in the computational environment of MATLAB (The Mathworks, Inc.). No assumptions regarding the spectroscopic responses of the different species are made through this process.

153 **DFT Calculations**

154 DFT+D calculations were performed using an ab initio plane-wave pseudopotential
155 approach as implemented in VASP.[22,23] The Perdew-Burke-Ernzerhof (PBE)
156 functional[24] was chosen to perform the periodic DFT calculations using the projector
157 augmented-wave method (PAW)[25] and a cutoff of 400 eV. The dispersion forces were
158 taken into account using the Grimme D2 approach.[26] To avoid the heavier
159 computational treatment of magnetic and electron-correlated iron oxides, we chose to
160 perform DFT calculations on two Al oxy-hydroxides (non-magnetic compounds): (i)
161 diaspore (α-AlOOH) which is the Al(III) isomorph of goethite, and (ii) gibbsite ($AlOH_3$)
162 because the co-binding phenomenon is experimentally shown on this mineral surface
163 (See SI). This allowed also to perform more extensive calculations.
164 The bulk gibbsite and bulk diaspore were optimized and a (2x2) and a (4x4) cell was
165 chosen to build the basal surfaces, respectively. Then the molecules were optimized
166 separately in the same supercell as that used to model the surface, and the dimer was
167 also studied. Several protonation states of the NFA were considered. Since the
168 determination of adsorption free energy from water phase was not the aim of our study,
169 the solvent water molecules were not included in the calculations. The adsorption
170 energies computed here inform rather on the molecule-surface interaction strength. The
171 detailed calculation results are detailed in the SI.
172

Results and Discussion

Macroscopic assessment of NA and NFA binding. Binding kinetics of NA and NFA in both single and binary systems followed pseudo-second-order kinetic model (Fig. S3) and displayed comparable behaviours, with NA binding more strongly than NFA. However, NFA loadings were considerably enhanced in the presence of NA, thus providing a first line of evidence for synergetic intermolecular interactions at mineral surfaces (SI). This can also be appreciated by ~4-fold slower adsorption rate of NFA in the mixed system (pseudo-second order rate constant of 0.16 $m^2/\mu mol \cdot min$) than in the isolated system (0.60 $m^2/\mu mol \cdot min$). In contrast, mixed systems containing SMX did not reveal any co-binding effects (Fig. S4).

NA and NFA binding at mineral surfaces in single system (Fig.1 for goethite) follows the typical pH-dependent behaviour of carboxylic acids.[10,27–29] NA adsorption was accordingly greatest under acid to circumneutral pH, where goethite surfaces are positively charged, and NA carboxylate groups deprotonated (pK_a =6.19 for NA at infinite dilution[30,] *cf.* Fig. S5). However, as NFA is a diprotic acid (pKa_1=2.28 and pKa_2=5.10 at infinite dilution)[31], it can exist as cationic, zwitterionic and anionic forms. Only 23% of NFA was sorbed at acid pH and this percentage decreased with pH increasing. Interestingly, binding of NA and NFA in mixed systems occurs over the entire pH 4-9 range considered in this work (Figs. 1). This cooperative effect is more pronounced for NFA because of its weaker adsorption in the isolated system (e.g. increase of adsorption from 22% to 54% at pH 5). In addition, the pH-adsorption curve of NFA (Fig.1b) becomes bell-shaped as in NA (Fig. 1a), suggesting that the NFA

195 binding to goethite surfaces in the binary system is closely related to the behavior of
196 NA binding.

197 Because this synergetic effect was observed for both molecules, two approaches
198 were adopted to study NFA and NA co-binding in mixed systems. Firstly, varying the
199 concentrations of NA and NFA, at ratio of 1:1 ($[NFA]_{tot} = [NA]_{tot}$), strongly points to
200 NA/NFA co-binding at goethite surfaces under a wide range of solute concentration
201 (0.1 to 40 μM), a range that notably partially overlaps with those in aquatic
202 environments (nM to several dozens of nM)[3–6] (Fig. 2a). Indeed, NFA and NA loadings
203 at pH 6 in isolated systems were lower than those measured in equimolar mixtures (Fig.
204 2a). Interestingly, by plotting the NFA loadings versus NA loadings in equimolar
205 mixtures, an excellent linear correlation was obtained (Fig. 2b, $[NFA]_{ads} = 0.6344$
206 $[NA]_{ads}$, $R^2 = 0.999$, fitted line was not shown). Secondly, varying $[NA]_{tot}$ at constant
207 $[NFA]_{tot}$ (20 μM) and, conversely, varying $[NFA]_{tot}$ at constant $[NA]_{tot}$ (20 μM) showed
208 that increasing surface loadings of one ligand increases the other. However, a plateau
209 was reached for $[NFA]_{ads}$ where $[NA]_{tot}$ varies, which is likely to have arisen from
210 molecular layers acting as steric or electrostatic barriers preventing additional
211 binding.[32]

212

213 **Molecular investigations of co-binding.** Vibration spectroscopy and density
214 functional theory (DFT) calculations were used to provide clues on the mechanisms
215 through which NA and NFA bind and co-bind at goethite surfaces. We note that DFT
216 calculations were performed on diaspore (Fig. 3), which is the Al(III) isomorph of

goethite, to avoid the otherwise heavier computational treatment of magnetic and electron-correlated iron oxides. The (110) face was chosen to emulate the dominant crystallographic face of the goethite particles under study.

The fingerprint region of these molecules (1200-1800 cm^{-1}; Fig. 4, see also band assignments in SI) showed a 25 cm^{-1} blue shifts in C-O stretching modes (ν_{COO}), while no obvious shift for the ring modes ν_{ring} was observed. This suggests direct interactions of carboxyl groups with goethite but little interaction with the aromatic and pyridine rings during the sorption of NA and NFA in single system[13,33]. Though vibration spectroscopy suggests both metal- and hydrogen-bonding for NA, DFT calculations suggest that hydrogen bonding is the preferred binding mode for NA (-0.34 eV *vs.* +0.44 eV for inner sphere complexation) and that it is 0.37 eV more favourable than NFA (+0.03 eV). Thus while both complexes are stabilised by direct hydrogen bonds between carboxyl groups and surface hydroxo groups, NA binding is made stronger by a vicinal carbonyl of the pyridine ring and involves a hydrogen-bond cycle between the molecule and two surface water molecules (Fig.3). In contrast, this cycle is not only absent in NFA but when we forcefully hydrogen bonded NFA with an adsorbed water simulations showed that this water reoriented itself towards a neighboring water molecule. The weak nature of NFA binding can even be compared to those of monocarboxylic acids (*e.g.* acetate or benzoate[13]).

238 Vibration spectra of mixed NA+NFA systems exposed to goethite (Fig. 4) showed
239 that increasing NFA concentrations (0, 10, 20, 50 and 100 μM) with $[NA]_{tot}$ = 100 μM
240 systematically increased the intensities of the characteristic bands of NFA
241 ($\nu_{COO,as}$=1480-1560 cm^{-1}), yet the resulting spectra cannot be represented as simple
242 linear combinations of the isolated goethite-NA and goethite-NFA systems (Fig. S7a).
243 For instance, the ring mode ($\nu_{C=C,ring}$) of NA was shifted from 1578 cm^{-1} to 1522 cm^{-1}
244 and that of NFA was split into two bands (1335 and 1348 cm^{-1}) suggesting perturbation
245 of C-C stretches and/or C-H bends of the aromatic and pyridine rings[34,35], and thus
246 formation of dimer involving the aromatic and pyridine rings of NFA and NA. These
247 observations also hold for the converse experiments where NA concentrations (0, 10,
248 20, 50 and 100 μM) are increased with $[NA]_{tot}$ = 100 μM (Fig. S7b).
249 A multivariate curve resolution (MCR) analysis[21] of these spectral sets provided
250 further insight into the nature of NFA and NA co-binding. MCR decomposed each
251 spectral sets into two separate spectral components (Figs. 5 a,b) representing the purest
252 extractable mineral-bound NFA and NA complexes (MCR I) and those under
253 competing systems (MCR II). The related concentration profiles (Fig. 5c) revealed that
254 addition of NA to mineral-bound NFA was more effective at altering the spectral
255 profile of NFA than the converse addition of NFA to mineral-bound NA. Still, as the
256 resulting MCR II components are markedly similar, our results suggest that the
257 resulting surface complexes at equimolar NA and NFA levels are strongly similar
258 irrespective of the order of addition. Finally, we note that these observations also hold
259 for lower concentrations (Fig. S8 where $[NA]_{tot}$ = 20 μM and $[NFA]_{tot}$=10-40 μM).

In line with the concept that NA enhances NFA binding, DFT calculations reveal that NFA binding to a hydrogen-bound NA on diaspore is energetically favourable (-0.21 eV). The resulting dimer formed via favourable hydrogen bonding and van der Waals interactions by -0.50 eV, and the two COOH moieties of this dimer are parallel with one another thus increasing the strengths of its interactions with mineral surfaces (*cf.* SI for more information and Figures S10-S15). As such, recalling that NA binding is favourable by -0.34 eV, binding of NFA to a pre-sorbed NA should be favourable by -0.55 eV. In comparison, NA and NFA binding at different locations on the same diaspore surface are favourable by only -0.30 eV and the formation an unbound NA/NFA dimer is favourable by -0.50 eV.

Because the main mode of attachment for NA is achieved via hydrogen bonding at circumneutral conditions, this phenomenon is not only limited to strongly reactive faces of minerals, such as the (110) face of goethite/diaspore or edges of clays, but also on the basal planes of minerals. The planes are of widespread occurrence in platy metal (oxy)(hydr)oxides as well as phyllosilicates (*e.g.* clays) and typically display (hydr)oxo groups that are strongly resilient to ligand exchange, yet are active hydrogen bonding sites. To illustrate this point further the SI contains further details on the energetics of NA/NFA co-binding on the basal plane of gibbsite, an important aluminium hydroxide in natural but also industrial settings. Gibbsite gives more weight to our demonstration, since the NA/NFA co-binding is experimentally shown to occur on this mineral surface (See Fig. S16).

Those results also fall precisely in line with those obtained for diaspore, and suggests the possibility in generalizing our finding to an even broader range of minerals and particles which capable of stabilizing NA-like molecules via hydrogen bonding. Our calculations consequently lend strong independent support for the concept that NA and NFA co-bind at mineral surfaces of even contrasting structure, and that a dimer-type species stabilized by intermolecular hydrogen bonding and van der Waals interactions could be responsible for this phenomenon.

Implications for transport of pharmaceutical compounds in nature. Our concerted macroscopic and molecular efforts both provide evidence that NFA-NA interactions mutually enhance binding at mineral surfaces such as goethite. This cooperative effect is more pronounced for NFA because of its intrinsically weaker affinity for mineral surfaces, and occurs under environmentally relevant conditions of drug concentration and pH. Vibration spectroscopic data show that addition of NA effectively alters the nature of mineral-NFA binding but that converse addition of NFA to mineral-bound NA results in a less dramatic change in the nature of NA binding. In support to these finding DFT calculations showed that NFA binding on mineral faces of even strongly contrasting structures is thermodynamically favoured only when NA is pre-adsorbed either metal-bonded or hydrogen-bonded. This favoured form of binding could be explained by the formation of a NFA-NA dimer stabilised by hydrogen bonding and van der Waals interactions. The lack of co-binding seen in SMX also suggests the

importance of understanding drug interactions in aqueous solutions, a finding that also calls for new studies along these lines.

This study is the first to show that mineral-bound antibiotic molecules can be specific adsorption sites for other antibiotic molecules, and that layered-like coatings involving anti-inflammatory agents may even form at mineral surfaces. As water resources are exposed to complex mixtures of chemicals[36], including natural organic matter and metal ions, additional efforts resolving the underlying principles governing cooperative sorption should be made to accurately assess the fate of co-existing contaminants in the environment. This becomes even more so urgent under the growing number aquatic ecosystems and groundwater systems exposed to emerging contaminants including non-prescription drugs, antibiotics, hormones and prescription drugs[36,37]. As a result, recognising the importance of drug co-binding at mineral surfaces, and the conditions where it does not occur such as in the case of SMX, is key to the successful development of models for predicting the fate of these contaminants, and for guiding policies on actions needed to mitigate this growing environmental problem.

Acknowledgements

This work was supported by Rennes Métropole and Région Bretagne (K.H). We gratefully acknowledge the Chinese Scholarship Council of PR China for providing financial support for Jing XU to stay at the ENSCR - Rennes University. Support to J.-F.B. was provided by the Swedish Research Council (2016-03808).

325 **Supporting Information Available**

326 Details of the materials used in this study, mineral characterization, analytical and DFT
327 methods, and additional data are available in the Supporting Information. This
328 information is available free of charge via the Internet at http://pubs.acs.org/.

329

330 **References**

331 (1) Lapworth, D. J.; Baran, N.; Stuart, M. E.; Ward, R. S. Emerging organic
332 contaminants in groundwater: a review of sources, fate and occurrence. *Environ.*
333 *Pollut.* **2012**, *163*, 287–303.

334 (2) Kolpin, D. W.; Furlong, E. T.; Meyer, M. T.; Thurman, E. M.; Zaugg, S. D.;
335 Barber, L. B.; Buxton, H. T. Pharmaceuticals, hormones, and other organic
336 wastewater contaminants in US streams, 1999-2000: A national reconnaissance.
337 *Environ. Sci. Technol.* **2002**, *36* (6), 1202–1211.

338 (3) Hernando, M. D.; Mezcua, M.; Fernández-Alba, A. R.; Barceló, D.
339 Environmental risk assessment of pharmaceutical residues in wastewater
340 effluents, surface waters and sediments. *Talanta* **2006**, *69* (2), 334–342.

341 (4) Heberer, T. Occurrence, fate, and removal of pharmaceutical residues in the
342 aquatic environment: a review of recent research data. *Toxicol. Lett.* **2002**, *131*
343 (1), 5–17.

344 (5) Fatta-Kassinos, D.; Meric, S.; Nikolaou, A. Pharmaceutical residues in
345 environmental waters and wastewater: Current state of knowledge and future
346 research. *Anal. Bioanal. Chem.* **2011**, *399* (1), 251–275.

347 (6) Gothwal, R.; Shashidhar, T. Antibiotic Pollution in the Environment: A Review.
348 *CLEAN--Soil, Air, Water* **2015**, *43* (4), 479–489.

349 (7) Gu, C.; Karthikeyan, K. G. Sorption of the antimicrobial ciprofloxacin to
350 aluminum and iron hydrous oxides. *Environ. Sci. Technol.* **2005**, *39* (23),
351 9166–9173.

(8) Wang, Y.; Newman, D. K. Redox reactions of phenazine antibiotics with ferric (hydr) oxides and molecular oxygen. *Environ. Sci. Technol.* **2008**, *42* (7), 2380–2386.

(9) Xu, X.-R.; Li, X.-Y. Sorption and desorption of antibiotic tetracycline on marine sediments. *Chemosphere* **2010**, *78* (4), 430–436.

(10) Paul, T.; Liu, J.; Machesky, M. L.; Strathmann, T. J. Adsorption of zwitterionic fluoroquinolone antibacterials to goethite: A charge distribution-multisite complexation model. *J. Colloid Interface Sci.* **2014**, *428*, 63–72.

(11) Pouliquen, H.; Le Bris, H. Sorption of oxolinic acid and oxytetracycline to marine sediments. *Chemosphere* **1996**, *33* (5), 801–815.

(12) Kulshrestha, P.; Giese, R. F.; Aga, D. S. Investigating the molecular interactions of oxytetracycline in clay and organic matter: insights on factors affecting its mobility in soil. *Environ. Sci. Technol.* **2004**, *38* (15), 4097–4105.

(13) Norén, K.; Persson, P. Adsorption of monocarboxylates at the water/goethite interface: The importance of hydrogen bonding. *Geochim. Cosmochim. Acta* **2007**, *71* (23), 5717–5730.

(14) Sun, D.; Zhang, X.; Wu, Y.; Liu, T. Kinetic mechanism of competitive adsorption of disperse dye and anionic dye on fly ash. *Int. J. Environ. Sci. Technol.* **2013**, *10* (4), 799–808.

(15) Conkle, J. L.; Lattao, C.; White, J. R.; Cook, R. L. Competitive sorption and desorption behavior for three fluoroquinolone antibiotics in a wastewater treatment wetland soil. *Chemosphere* **2010**, *80* (11), 1353–1359.

(16) Xing, B.; Pignatello, J. J. Competitive sorption between 1, 3-dichlorobenzene or 2, 4-dichlorophenol and natural aromatic acids in soil organic matter. *Environ. Sci. Technol.* **1998**, *32* (5), 614–619.

(17) Jones-Lepp, T. L.; Alvarez, D. A.; Englert, B.; Batt, A. L. Pharmaceuticals and Hormones in the Environment. *Encycl. Anal. Chem.* **2009**.

(18) Zhang, T.; Li, B. Occurrence, Transformation, and Fate of Antibiotics in Municipal Wastewater Treatment Plants. *Crit. Rev. Environ. Sci. Technol.* **2011**, *41* (11), 951–998.

(19) Jagtap, S.; Yenkie, M. K.; Labhsetwar, N.; Rayalu, S. Fluoride in drinking water and defluoridation of water. *Chem. Rev.* **2012**, *112* (4), 2454–2466.

(20) Marsac, R.; Martin, S.; Boily, J.-F.; Hanna, K. Oxolinic acid binding at goethite and akaganéite surfaces: implications for aquaculture-induced pollution. *Environ. Sci. Technol.* **2016**, *50* (2), 660–668.

(21) Jaumot, J.; Gargallo, R.; de Juan, A.; Tauler, R. A graphical user-friendly interface for MCR-ALS: a new tool for multivariate curve resolution in MATLAB. *Chemom. Intell. Lab. Syst.* **2005**, *76* (1), 101–110.

(22) Kresse, G.; Hafner, J. Ab initio molecular dynamics for liquid metals. *Phys. Rev. B* **1993**, *47* (1), 558–561.

(23) Kresse, G.; Hafner, J. Norm-conserving and ultrasoft pseudopotentials for first-row and transition elements. *J. Phys. Condens. Matter* **1994**, *6* (40), 8245.

(24) Perdew, J. P.; Burke, K.; Ernzerhof, M. Generalized gradient approximation made simple. *Phys. Rev. Lett.* **1996**, *77* (18), 3865–3868.

(25) Blöchl, P. E. Projector augmented-wave method. *Phys. Rev. B* **1994**, *50* (24), 17953–17979.

(26) Grimme, S.; Antony, J.; Ehrlich, S.; Krieg, H. A consistent and accurate ab initio parametrization of density functional dispersion correction (DFT-D) for the 94 elements H-Pu. *J. Chem. Phys.* **2010**, *132* (15), 154104.

(27) Rusch, B.; Hanna, K.; Humbert, B. Sorption and transport of salicylate in a porous heterogeneous medium of silica quartz and goethite. *Environ. Sci. Technol.* **2010**, *44* (7), 2447–2453.

(28) Paul, T.; Machesky, M. L.; Strathmann, T. J. Surface complexation of the zwitterionic fluoroquinolone antibiotic ofloxacin to nano-anatase TiO2 photocatalyst surfaces. *Environ. Sci. Technol.* **2012**, *46* (21), 11896–11904.

(29) Pei, Z.; Shan, X. Q.; Kong, J.; Wen, B.; Owens, G. Coadsorption of ciprofloxacin and Cu(II) on montmorillonite and kaolinite as affected by solution pH. *Environ. Sci. Technol.* **2010**, *44* (3), 915–920.

(30) Ross, D. L.; Riley, C. M. Aqueous solubilities of some variously substituted quinolone antimicrobials. *Int. J. Pharm.* **1990**, *63* (3), 237–250.

(31) Takács-Novák, K.; Tam, K. Y. Multiwavelength spectrophotometric determination of acid dissociation constants: Part V: microconstants and tautomeric ratios of diprotic amphoteric drugs. *J. Pharm. Biomed. Anal.* **2000**, *21* (6), 1171–1182.

(32) Liu, S. Cooperative adsorption on solid surfaces. *J. Colloid Interface Sci.* **2015**, *450*, 224–238.

(33) Madey, T. E.; Yates Jr, J. T. *Vibrational spectroscopy of molecules on surfaces*; Springer Science & Business Media, 2013; Vol. 1.

(34) Akyuz, S.; Akyuz, T. FT-IR spectroscopic investigations of adsorption of 2-, 3-and 4-pyridinecarboxamide on montmorillonite and saponite from Anatolia. *Vib. Spectrosc.* **2006**, *42* (2), 387–391.

(35) Balci, K.; Akkaya, Y.; Akyuz, S. An experimental and theoretical vibrational spectroscopic study on niflumic acid, a non-steroidal anti-inflammatory drug. *Vib. Spectrosc.* **2010**, *53* (2), 239–247.

(36) Schwarzenbach, R. P.; Escher, B. I.; Fenner, K.; Hofstetter, T. B.; Johnson, C. A.; von Gunten, U.; Wehrli, B. The challenge of micropollutants in aquatic systems. *Science* **2006**, *313* (5790), 1072–1077.

(37) Rotter, S.; Gunold, R.; Mothes, S.; Paschke, A.; Brack, W.; Altenburger, R.; Schmitt-Jansen, M. Pollution-Induced Community Tolerance To Diagnose Hazardous Chemicals in Multiple Contaminated Aquatic Systems. *Environ. Sci. Technol.* **2015**, *49* (16), 10048–10056.

435 **Figure captions**

436

437 **Figure1.** Left: pH-adsorption edges of a) NA single ($[NA]_{tot}$ = 20 μM) and binary
438 ($[NA]_{tot}$ = $[NFA]_{tot}$ = 20 μM) and b) NFA single ($[NFA]_{tot}$ = 20 μM) and binary
439 ($[NFA]_{tot}$ = 20 μM; $[NA]_{tot}$ = 10 and 20 μM) systems on goethite, with 10 mM NaCl.
440 Right: molecular structures of NA and NFA.

441 **Figure 2.** a) NA and NFA sorption to goethite for single systems (full symbols) and
442 binary system where $[NA]_{tot}$ = $[NFA]_{tot}$ (empty symbols). NA and NFA concentrations
443 were varied from 0.1 to 40 μM. For the sake of readability, the behaviour at very low
444 concentrations was shown in the insert. b) $[NFA]_{ads}$ vs $[NA]_{ads}$ at three experimental
445 conditions: (i) varying both compounds from 0 to 40 μM (black), (ii)$[NFA]_{tot}$ = 20 μM,
446 $0 < [NA]_{tot} < 40$ μM (red), and (iii) $[NA]_{tot}$ = 20 μM, $0 < [NFA]_{tot} < 40$ μM (blue).

447 **Figure 3.** NA and NFA molecules co-adsorbed on the diaspore surface, with NA
448 adsorbed as (*left*) inner sphere (E_{ads} (NFA/NA) = 0.07 eV, athermic process) and (*right*)
449 outer sphere (E_{ads} (NFA/NA) = -0.21 eV). A negative energy indicates an exothermic
450 process.

451 **Figure 4.** ATR-FTIR spectroscopy on goethite. (a) from top to bottom: NA single
452 system, dissolved NA ($NA_{(aq)}$ in 1 M NaOH), NA-NFA binary system ($[NA]_{tot}$ = 100
453 μM, $10 < [NFA]_{tot} < 100$ μM; the arrows show increasing $[NFA]_{tot}$), NFA single system,
454 dissolved NFA ($NFA_{(aq)}$ in 1 M NaOH). Bold and thin dashed lines show characteristic
455 bands of $NA_{(aq)}$ and $NFA_{(aq)}$, respectively. Numbers denote $[NFA]_{tot}$. Spectra were
456 normalized according to the band at 1448 cm^{-1}, since NA is the major component.

457 **Figure 5.** MCR-extracted spectral profiles from FTIR spectra of (a)100 μm NFA + NA ,
458 (b) 100 μm NA + NFA, both including reference spectra, and (c) associated
459 concentration profiles corresponding to components MCR I and II. These concentration
460 profiles underscore the larger propensity of NA at displacing bound NFA, than NFA at
461 displacing NA.
462

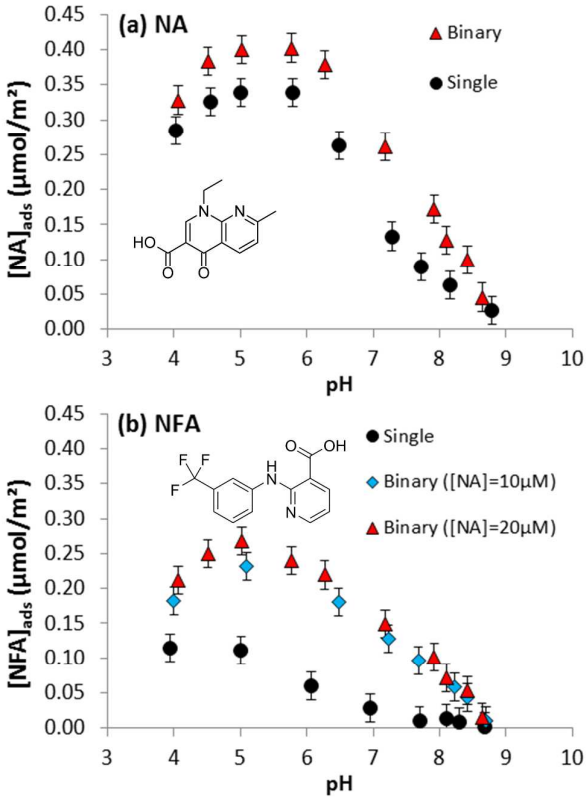
(a) NA
Binary
Single
[NA]ads (μmol/m²)
pH
(b) NFA
Single
Binary ([NA]=10μM)
Binary ([NA]=20μM)
[NFA]ads (μmol/m²)
pH

Figure 1

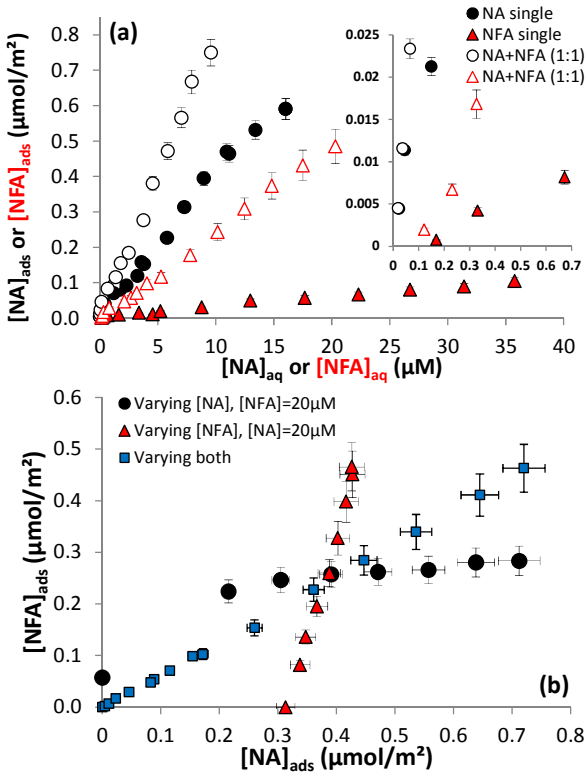
(a)
NA single
NFA single
NA+NFA (1:1)
NA+NFA (1:1)
[NA]ads or [NFA]ads (µmol/m²)
[NA]aq or [NFA]aq (µM)
Varying [NA], [NFA]=20µM
Varying [NFA], [NA]=20µM
Varying both
[NFA]ads (µmol/m²)
[NA]ads (µmol/m²)
(b)

Figure 2

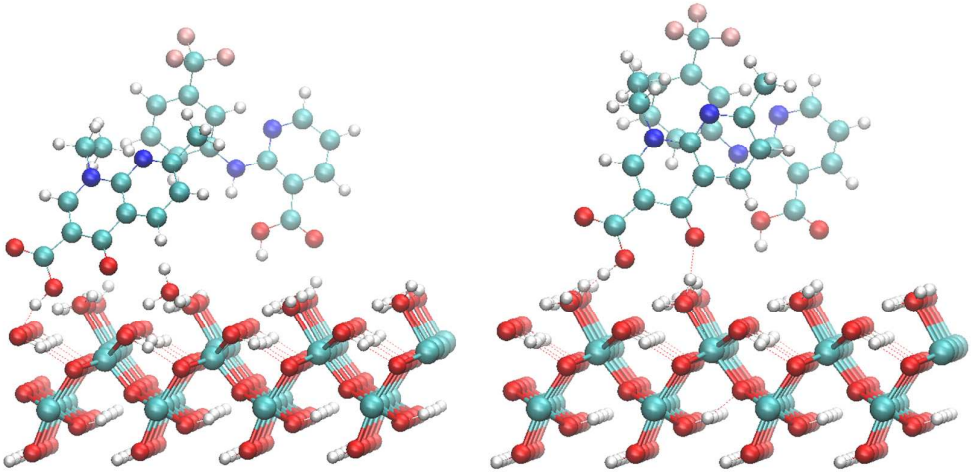

Figure 3

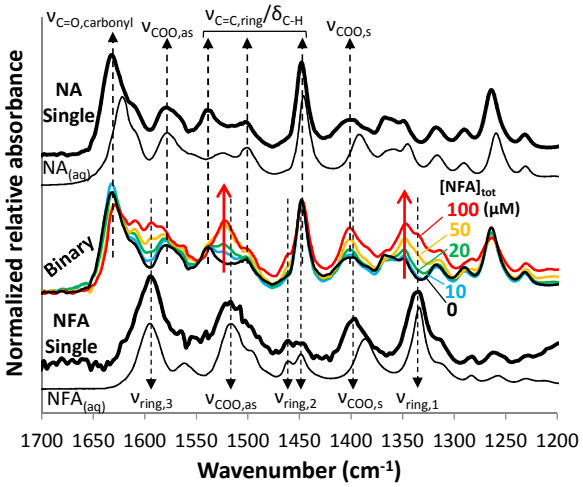

476

477 **Figure 4**

478

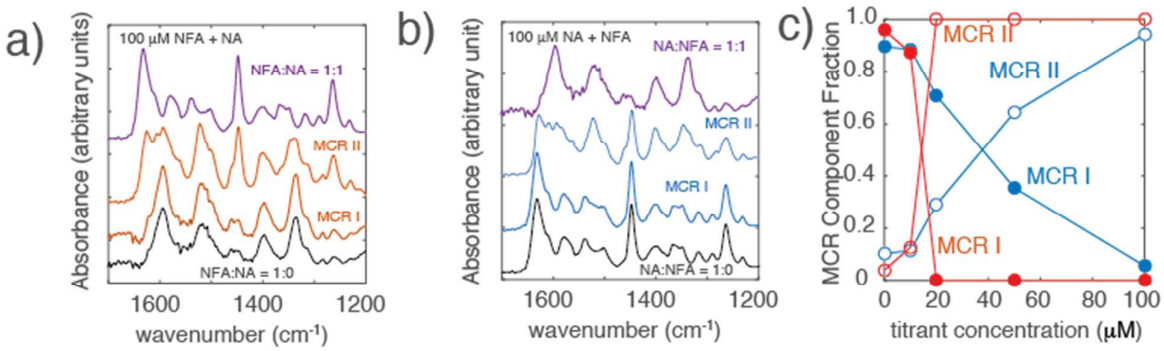
a)
100 μM NFA + NA
NFA:NA = 1:1
MCR II
MCR I
NFA:NA = 1:0
Absorbance (arbitrary units)
1600
1400
1200
wavenumber (cm-1)
b)
100 μM NA + NFA
NA:NFA = 1:1
MCR II
MCR I
NA:NFA = 1:0
Absorbance (arbitrary unit)
1600
1400
1200
wavenumber (cm-1)
c)
MCR II
MCR II
MCR I
MCR I
MCR Component Fraction
1.0
0.8
0.6
0.4
0.2
0
0
20
40
60
80
100
titrant concentration (μM)

Figure 5

482 **TOC**

483

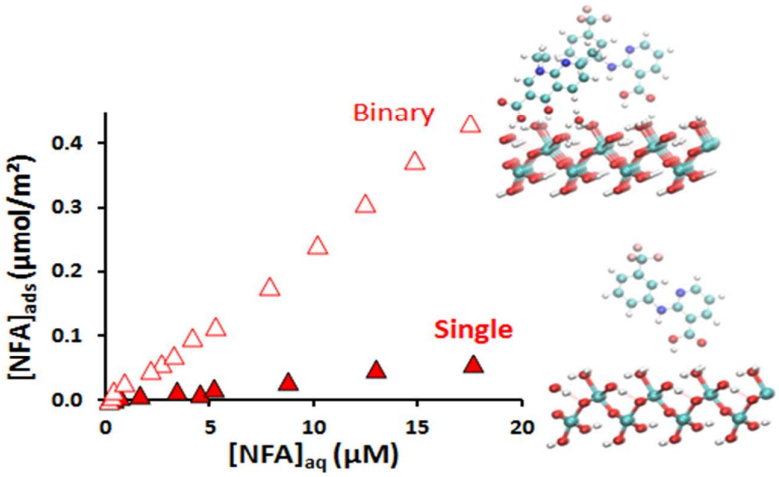

484